

**Angular momentum population in the projectile fragmentation of  $^{238}\text{U}$  at 750 MeV/nucleon**

K. A. Gladnishki,<sup>1,2</sup> Zs. Podolyák,<sup>1,\*</sup> P. H. Regan,<sup>1</sup> J. Gerl,<sup>3</sup> M. Hellström,<sup>3,4</sup> Y. Kopatch,<sup>3</sup> S. Mandal,<sup>3</sup> M. Górska,<sup>3</sup> R. D. Page,<sup>5</sup> H. J. Wollersheim,<sup>3</sup> A. Banu,<sup>3</sup> G. Benzoni,<sup>6</sup> H. Boardman,<sup>5</sup> M. La Commara,<sup>7</sup> J. Ekman,<sup>4</sup> C. Fahlander,<sup>4</sup> H. Geissel,<sup>3</sup> H. Grawe,<sup>3</sup> E. Kaza,<sup>3</sup> A. Korgul,<sup>8</sup> M. Matos,<sup>3</sup> M. N. Mineva,<sup>4</sup> C. J. Pearson,<sup>1</sup> C. Plettner,<sup>3</sup> D. Rudolph,<sup>4</sup> Ch. Scheidenberger,<sup>3</sup> K.-H. Schmidt,<sup>3</sup> V. Shishkin,<sup>3</sup> D. Sohler,<sup>9</sup> K. Sümmerer,<sup>3</sup> J. J. Valiente-Dobón,<sup>1</sup> P. M. Walker,<sup>1</sup> H. Weick,<sup>3</sup> M. Winkler,<sup>3</sup> and O. Yordanov<sup>3</sup>

<sup>1</sup>*Department of Physics, University of Surrey, Guildford GU2 7XH, United Kingdom*

<sup>2</sup>*Faculty of Physics, University of Sofia, BG-1164 Sofia, Bulgaria*

<sup>3</sup>*GSI, Planckstrasse 1, D-64291 Darmstadt, Germany*

<sup>4</sup>*Department of Physics, Lund University, S-22100 Lund, Sweden*

<sup>5</sup>*Department of Physics, University of Liverpool, Liverpool L69 7ZE, United Kingdom*

<sup>6</sup>*Dipartimento di Fisica and INFN, Sezione di Milano, I-20133 Milano, Italy*

<sup>7</sup>*Department of Physics, University of Napoli, Napoli, Italy*

<sup>8</sup>*Institute of Experimental Physics, Warsaw University, Warsaw, Poland*

<sup>9</sup>*Institute of Nuclear Research, Debrecen, Hungary*

(Received 4 November 2003; published 27 February 2004)

A systematic study of the population probabilities of nanosecond and microsecond isomers produced following the projectile fragmentation of  $^{238}\text{U}$  at 750 MeV/nucleon has been undertaken at the SIS/FRS facility at GSI. Approximately 15 isomeric states in neutron-deficient nuclei around  $A \sim 190$  were identified and the corresponding isomeric ratios determined. The results are compared with a model based on the statistical abrasion-ablation description of relativistic fragmentation and simple assumptions concerning  $\gamma$  cascades in the final nucleus (sharp cutoff). This model represents an upper limit for the population of isomeric states in relativistic projectile fragmentation. When the decay properties of the states above the isomer are taken into account, as opposed to the sharp cutoff approximation, a good agreement between the experimental and calculated angular momentum population is obtained.

DOI: 10.1103/PhysRevC.69.024617

PACS number(s): 25.70.Mn, 23.20.-g

**I. INTRODUCTION**

During the last decade the application of projectile fragmentation reactions at intermediate and relativistic energies to studies of nuclei far from stability has made significant progress. One of the advantageous features of fragmentation reactions is the relatively high probability for populating high-spin isomeric states [1–4]. The combination of sensitivity and universality offered by projectile fragment separators, together with efficient, delayed  $\gamma$ -ray spectroscopy of the selected and identified ions in metastable states, gives good possibilities for obtaining nuclear structure information on very exotic nuclei far from stability [2,3,5–9].

The basic properties of fragmentation reactions, such as the production cross sections and momentum distributions of the reaction products, knowledge of which are crucial for the design and optimal operation of a fragment separator, are rather well known [10–12]. By contrast, experimental information on the population of states as a function of angular momentum in fragmentation reactions is much more scarce, particularly for projectile energies above 100A MeV. According to our knowledge, the first information regarding the population of isomeric states after projectile fragmentation at relativistic energies was presented by Schmidt-Ott *et al.* for  $^{43}\text{Sc}$  populated in the fragmentation of a 500A MeV  $^{46}\text{Ti}$

beam [1]. Recently, Pfützner *et al.* published isomeric ratios predominantly for heavy nuclei close to the stability line, populated in the fragmentation of  $^{238}\text{U}$  [3] and  $^{208}\text{Pb}$  [4]. In Ref. [4]  $\approx 20$  isomeric states were identified, mainly in near stable rare-earth and transitional nuclei with  $A \sim 180$ , and the corresponding isomeric ratios deduced.

Here we present the first systematic study on the angular momentum population in relativistic projectile fragmentation for neutron-deficient nuclei. Fifteen previously reported isomers have been identified in this work; their isomeric ratios were deduced and compared with theoretical calculations.

**II. EXPERIMENTAL DETAILS**

Neutron-deficient nuclei in the  $A \sim 190$  region were populated following the projectile fragmentation of a 750A MeV  $^{238}\text{U}$  primary beam impinging on a 1.6 g/cm<sup>2</sup> natural beryllium target. The primary beam with an intensity of  $4 \times 10^7$  in a 10 s spill was provided by the GSI heavy-ion synchrotron (SIS). The fragment separator (FRS) [13], which is a magnetic zero-degree spectrometer with two dipole stages, was used to separate the nuclei of interest. The FRS was operated in the standard achromatic mode with an aluminum degrader at the intermediate focal plane. Niobium foils of thicknesses 221 mg/cm<sup>2</sup> and 108 mg/cm<sup>2</sup> were placed after both the target and degrader positions, respectively, in order to maximize the electron stripping.

A schematic view of the experimental setup is shown in

\*Corresponding author. Email address: Z.Podolyak@surrey.ac.uk

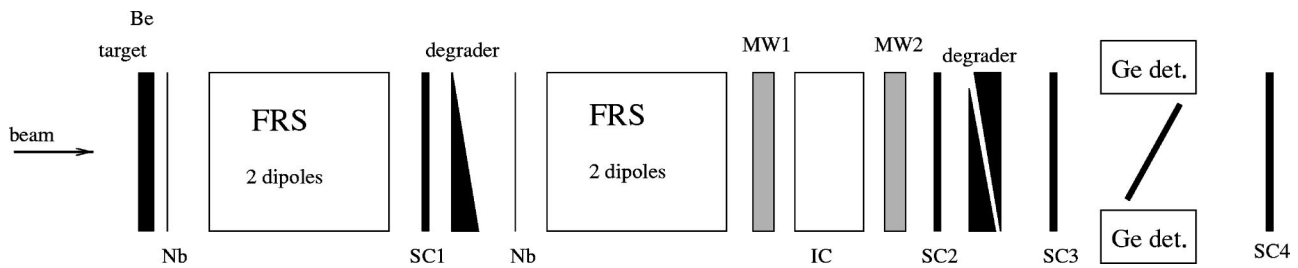


FIG. 1. Schematic view of the experimental setup. For details see the text.

Fig. 1. The time of flight through the second stage of the FRS was measured using scintillator detectors SC1 and SC2. The scintillator detector in the intermediate focal plane (SC1) was also used for position measurement. At the final focal plane the ions were tracked using two multiwire detectors MW1 and MW2. The time-of-flight and flightpath information were used to determine the mass-to-charge ratio of the ions [4]. The energy loss, providing  $Z$  information, was determined by a fourfold ionization chamber (MUSIC). An aluminum degrader of variable thickness was used to slow down the fragments of interest and ensure their implantation into a catcher. In contrast to our previous experiments with an aluminum catcher [14,15], a plastic catcher was used as it produces less prompt radiation during the slowing down process of the ions. Scintillator detectors placed both before (SC3) and after (SC4) the catcher were used to control the implantation of the ions.

The catcher was viewed by two segmented germanium Clover (VEGA) [16] detectors, in order to record the  $\gamma$  rays emitted from isomeric decays in the implanted ions. One of the crystals had rather poor energy resolution, so only seven crystals were used in the off-line analysis. The efficiency of the array was 5% at a  $\gamma$ -ray energy of 500 keV, as measured with a  $^{152}\text{Eu}$  point source placed in the middle of the catcher. The delay of  $\gamma$  rays with respect to the implantation time of a corresponding heavy ion was measured in two time ranges, 0–8  $\mu\text{s}$  and 0–80  $\mu\text{s}$ .

The method is sensitive to isomers with half-lives in the range from about 100 ns up to several milliseconds. The lower limit is determined by the time of flight through the FRS ( $\sim 300$  ns). However, as reported previously, if the electron conversion branch is blocked, as it is for highly stripped ions, the effective ionic lifetime in flight is increased, allowing shorter neutral atom decay half-lives to be measured [17,18]. The upper limit is determined by the need to correlate the individual ions to the delayed  $\gamma$  rays.

### III. DATA ANALYSIS

#### A. Ion identification

The ion identification procedure applied consists of three steps. The first step comes from the mass-to-charge ratio  $A/q$  versus position in the intermediate focal plane matrix, as shown in Fig. 2(a). The two structures correspond to nuclei which do not change charge state in the degrader and those which pick up one electron, respectively. The charge state distribution was calculated with the code GLOBAL [19]. It was estimated that the probability of an ion being fully

stripped is 85% in the first stage of the FRS. In the second stage, after the degrader, the probabilities of an ion being fully stripped and H-like are 57% and 36%, respectively. Therefore, the majority of the nuclei which do not change

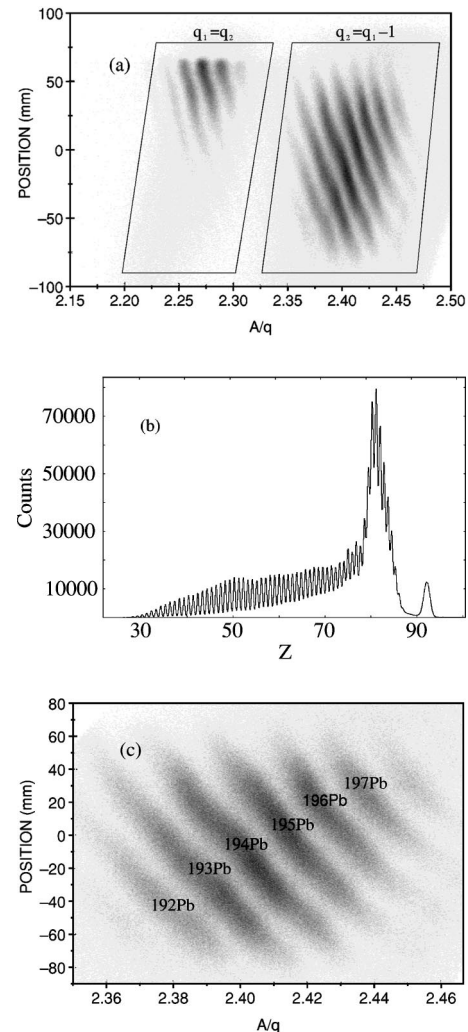


FIG. 2. Example of the ion identification procedure. A sample of the full statistics is shown. (a) Position of the ions in the middle of the FRS vs  $A/q$ . The parallelograms show the selection of events which do not change charge state in the middle of FRS and those which pick up one electron, respectively. (b) Spectrum of  $Z$  as measured by the ionization chamber. (c) Position in the middle of FRS vs  $A/q$  for Pb ions selected in (a) and (b). While there is a good separation between different isotopes, each ion with mass  $A$  and atomic number  $Z$  is contaminated by nuclear species with  $A+2$  and  $Z+1$ .

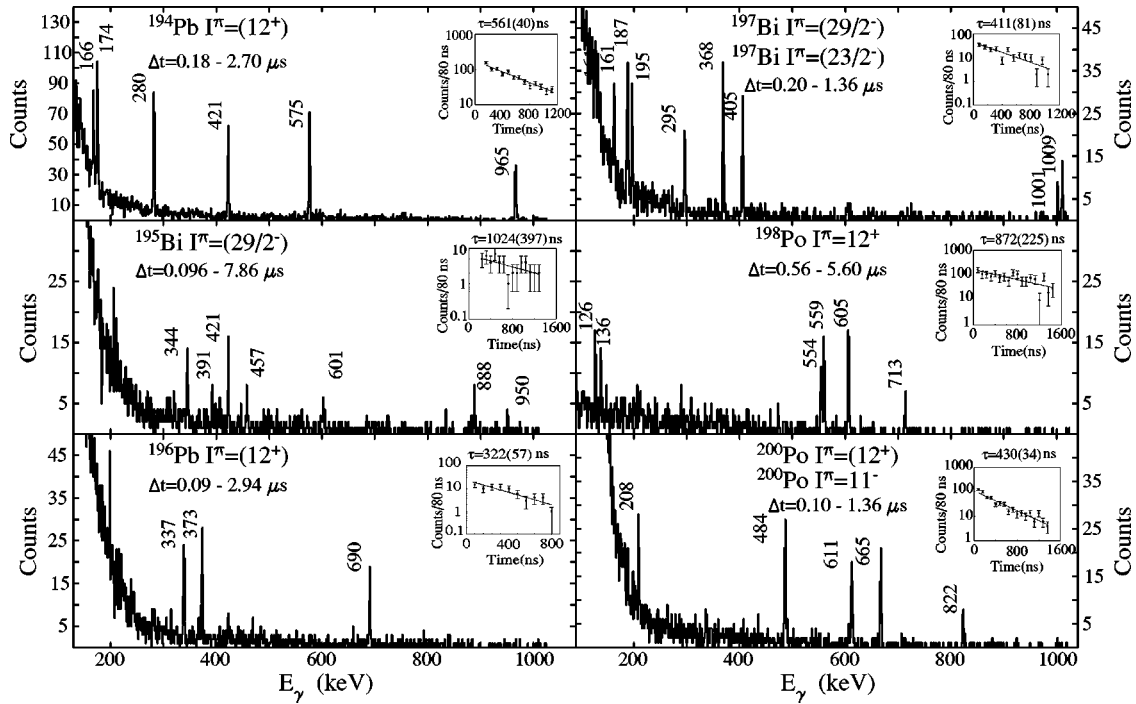


FIG. 3. Delayed  $\gamma$ -ray spectra associated with  $^{194}\text{Pb}$ ,  $^{195}\text{Bi}$ ,  $^{196}\text{Pb}$ ,  $^{197}\text{Bi}$ ,  $^{198}\text{Po}$ , and  $^{200}\text{Po}$ . The time spectra with fitted mean lifetimes are given in the insets. The  $\gamma$  rays labeled with an asterisk in  $^{195}\text{Bi}$  are transitions observed for the first time in the present experiment.

their charge state are fully stripped in both stages of the FRS. Similarly, the predominant part of those nuclei which pick up one electron is fully stripped in the first stage and H-like in the second stage of the separator.

The FRS was nominally set to the central transmission of  $^{186}\text{Pb}$ , therefore the ions labeled with  $q_1=q_2$  in Fig. 2(a) are nuclei in the region of  $^{186}\text{Pb}$ . The nuclei transmitted as H-like ions in the second stage of the FRS are nuclei around  $^{194}\text{Pb}$ . Although the majority of a given species are transmitted as fully stripped, as predicted by the GLOBAL calculations, Fig. 2(a) shows that a larger number of ions are actually H-like. This is due to the much larger production cross section of nuclei around  $^{194}\text{Pb}$  compared with those around  $^{186}\text{Pb}$ . Cross section measurements of the fragmentation of 1A GeV  $^{238}\text{U}$  beam on a deuterium target indicate a ratio of  $\sigma(^{194}\text{Pb})/\sigma(^{186}\text{Pb}) \gg 100$  [20]. All the isomers observed in the current work are in nuclei transmitted as fully stripped in the first stage and H-like in the second stage of FRS, in a single setting. No isomeric states were identified in nuclei around the fully stripped  $^{186}\text{Pb}$  in the current work, presumably because of low statistics and/or isomeric lifetimes for which the technique is not sensitive.

In the second step of the identification procedure a gate was applied on the Z spectrum obtained from the energy loss in the ionization chamber MUSIC. As can be seen in Fig. 2(b), the Z resolution is not good enough to separate neighboring elements cleanly.

After the charge state and Z selection a new matrix of  $A/q$  versus position in the intermediate focal plane was created for each element, as shown in Fig. 2(c). In this way a good separation could be obtained between the different isotopes of a given element. However, each mass A of an element with atomic number Z,  $^A_Z X$ , was contaminated with  $^{A+2}_{Z+1} Y$  nu-

clei. The level of contamination is relevant for the determination of the isomeric ratio, and therefore is discussed later in Sec. III C.

Note that the identification procedure described above is slightly different from the standard one (see, e.g., Ref. [4]). The standard identification procedure could not be used due to the poor position resolution obtained for the incoming ions at the final focal plane.

### B. Delayed $\gamma$ spectra

$\gamma$ -ray energy versus delay time matrices were created for each species. The matrices were projected on the two axes to achieve quantitative energy and time information. Examples of delayed  $\gamma$ -ray spectra corresponding to different nuclei are shown in Fig. 3.

### C. Experimental isomeric ratio

The isomeric ratio  $R$  is defined as the probability that in the reaction a nucleus is produced in an isomeric state. It was determined as outlined below [4]. The observed decay yield  $Y$  is calculated using the following expression:

$$Y = \frac{N_\gamma(1 + \alpha_{tot})}{\epsilon_{eff} b_\gamma}, \quad (1)$$

where  $N_\gamma$  is the number of counts in the  $\gamma$ -ray line depopulating the isomer of interest,  $\alpha_{tot}$  is the total conversion coefficient for this transition,  $b_\gamma$  is the absolute  $\gamma$ -ray branching ratio, and  $\epsilon_{eff}$  is the  $\gamma$ -ray detection efficiency. Among these quantities, the determination of the efficiency is not straightforward. Since different nuclei were implanted at different locations in the  $\approx 20$  cm long catcher, the dependence of

$\gamma$ -ray detection efficiency on the horizontal position must be deduced. Therefore the efficiency was measured by placing a calibration source at three different positions, and the efficiencies used for different species were interpolated from these. The slowing down and stopping of heavy ions in the catcher were accompanied by a prompt burst of radiation, mainly due to bremsstrahlung [15,21]. Since the gate for  $\gamma$ -ray detection allowed the recording of prompt radiation and only the first  $\gamma$  ray in every channel was recorded in an event, the effective efficiency for delayed radiation was reduced. In this way the efficiency was reduced by about 30% (which corresponds to approximately two crystals out of seven being hit by the prompt radiation). The number of crystals detecting prompt radiation, and therefore the corresponding efficiency lost, was determined for each nuclear species separately.

The isomeric ratio is given by

$$R = \frac{Y}{N_{imp}FG}, \quad (2)$$

where  $N_{imp}$  is the number of implanted heavy ions.  $F$  and  $G$  are correction factors for the in-flight isomer decay losses and the finite detection time of the  $\gamma$  radiation, respectively. These two quantities are calculated as

$$F = \exp\left[-\left(\lambda^{q_1} \frac{TOF_1}{\gamma_1} + \lambda^{q_2} \frac{TOF_2}{\gamma_2}\right)\right], \quad (3)$$

$$G = \exp(-\lambda t_i) - \exp(-\lambda t_f), \quad (4)$$

where  $TOF_1$  ( $TOF_2$ ) is the time of flight through the first (second) stage of FRS,  $\gamma_1$  ( $\gamma_2$ ) is the corresponding Lorentz factor, and  $\lambda^{q_1}$  ( $\lambda^{q_2}$ ) is the decay constant for the ion in the charge state  $q_1$  ( $q_2$ ).  $TOF_1$  and  $\gamma_1$  were calculated using the code MOCADI [22].  $TOF_2$  was measured in the experiment and was approximately 160 ns.  $t_i$  and  $t_f$  are the  $\gamma$  delay-time limits set in the off-line analysis to produce the delayed  $\gamma$  spectrum. For fully stripped ions, the decay constant  $\lambda^0$  can be calculated with the following equation:

$$\lambda^0 = \lambda \sum_i \frac{b_i \gamma_i}{1 + \alpha_{tot}^i}, \quad (5)$$

where the summation is over all the decay branches depopulating the isomer.

When more than one isomer in the same nucleus is populated in the reaction a lower-lying isomer may be partly fed by the delayed decay of a higher-lying metastable state. We use the definition of isomeric ratio as the probability that a state is populated promptly after production of the nucleus in the reaction (as in Ref. [4]). If the upper metastable state decays with the probability (branching)  $b_{UL}$  to the lower one, the isomeric ratio for the lower isomer can be calculated by

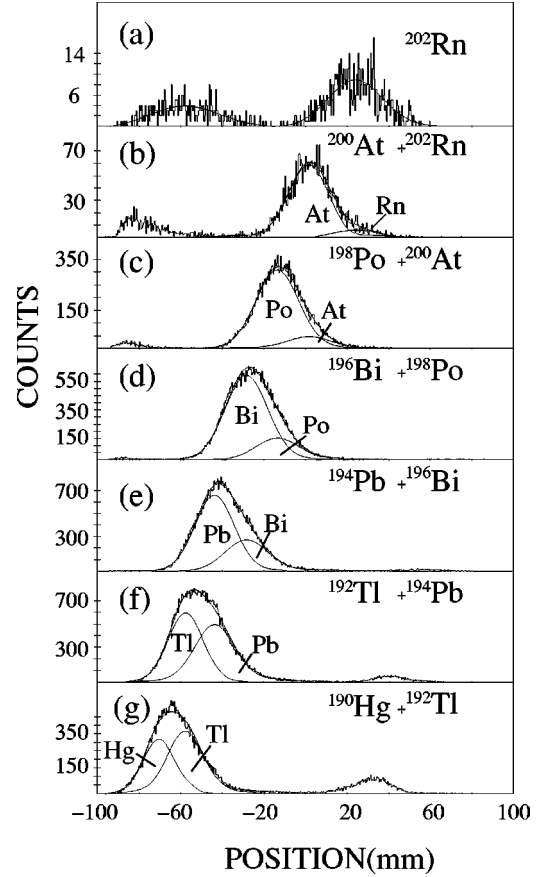


FIG. 4. Samples of position spectra at the final focal plane of the separator. They illustrate the applied procedure to separate the nucleus of interest from the contamination, as described in the text.

$$R_L = \frac{Y_L}{N_{imp}F_L G_L} - b_{UL} \frac{R_U}{F_L G_L} \left[ \frac{\lambda_U (G_U - G_L)}{\lambda_L - \lambda_U} F_U + \frac{\lambda_U^0}{\lambda_L^0 - \lambda_U^0} G_L (F_U - F_L) \right], \quad (6)$$

where the indices “L” and “U” correspond to the lower- and the upper-lying isomeric states, respectively, and the second term on the right side represents the correction due to feeding from the upper state. We note that the above formula differs slightly from that given in our previous work [4] and corrects a minor error.

The majority of the quantities needed to determine the isomeric ratio arise from the knowledge of the level scheme (literature) and simple experimental considerations. However, the extraction of the number of implanted ions is more complex due to the contamination. As mentioned before, the  ${}^A_Z X$  ions are contaminated with  ${}^{A+2}_{Z+1} Y$  nuclei. In order to determine the level of contamination, the position at the final focal plane spectrum is examined. These spectra are obtained after gating on the individual isotopes of Fig. 2(c). Samples are shown in Fig. 4. Figure 4(a) presents the position spectrum corresponding to  ${}^{202}_{86} \text{Rn}$ . This nucleus is not contaminated, since no  $Z=87$  nuclei were transmitted through the FRS. The bigger peak corresponds to the H-like ions and is

TABLE I. List of isomers analyzed in the current work. For each nucleus the spin-parity, excitation energy, mean lifetime from the present work and literature, and experimental and theoretical isomeric ratios are given. Theoretical isomeric ratios are calculated both with the analytical formula and the ABRABLA code, in the sharp cutoff approximation. For details see the text.

Isotope	$I^\pi$	$E_{lev}$ (keV)	$\tau$ (Present work)	$\tau$ (Published value)	$R_{exp}$	$\rho_{th}$ Formula	$\rho_{th}$ ABRABLA
$^{188}\text{Hg}$	(12 <sup>+</sup> )	2724	270(51) ns	193(22) ns [33]	0.062 (19)	0.443	0.341
$^{192}\text{Tl}$	(8 <sup>-</sup> )	407+x	451(64) ns	427(7) ns [34]	0.22 (10)	0.666	0.569
$^{192}\text{Pb}$	(12 <sup>+</sup> )	2625	2.1( $_{-1.1}^{+\infty}$ ) $\mu\text{s}$	1.59 (7) $\mu\text{s}$ [34]	0.14 (3)	0.415	0.282
$^{193}\text{Pb}$	(33/2 <sup>+</sup> )	2613+x	104( $_{-34}^{+370}$ ) ns	194( $_{22}^{+36}$ ) ns [35]	0.015 (4)	0.190	0.113
$^{194}\text{Pb}$	(12 <sup>+</sup> )	2629	561(40) ns	505(14) ns [36]	0.16 (4)	0.400	0.280
$^{195}\text{Pb}$	21/2 <sup>-</sup>	1759	14.8( $_{-5.8}^{+130}$ ) $\mu\text{s}$	14.4(1) $\mu\text{s}$ [37]	0.150 (28)	0.484	0.407
$^{195}\text{Bi}$	(29/2 <sup>-</sup> )	2311+x	1.02(40) $\mu\text{s}$	1.08(7) $\mu\text{s}$ [37]	0.045 (9)	0.259	0.153
$^{196}\text{Pb}$	(12 <sup>+</sup> )	2694	322(57) ns	390(6) ns [38]	0.17 (4)	0.384	0.278
	(5 <sup>-</sup> )	1798		202(20) ns [38]	0.5 (3)	0.832	0.715
$^{197}\text{Bi}$	(29/2 <sup>-</sup> )	2360+x	411(81) ns	379(19) ns [39]	0.08 (2)	0.244	0.165
$^{198}\text{Po}$	12 <sup>+</sup>	2692+x	872(225) ns	1080(70) ns [40]	0.089 (12)	0.367	0.200
$^{200}\text{Po}$	(12 <sup>+</sup> )	2805+x	430 (34) ns	387(4) ns [41]	0.067 (12)	0.349	0.222
	11 <sup>-</sup>	2597		151(11) ns [41]	0.393 (41)	0.410	0.275
$^{202}\text{Po}$	(8 <sup>+</sup> )	(1714)		123(22) ns [42]	0.045 (12)	0.600	0.498

fitted with a Gaussian. In the next step the position spectrum of  $^{200}_{58}\text{At}$  is analyzed [Fig. 4(b)]. The peak is fitted with two Gaussians, one for  $^{202}\text{Rn}$  (with fixed position and width taken from the previous  $^{202}\text{Rn}$  spectrum) and the other for  $^{200}\text{At}$ . In the subsequent steps the  $^{198}\text{Po}$ ,  $^{196}\text{Bi}$ ,  $^{194}\text{Pb}$ , and  $^{192}\text{Tl}$  position spectra are examined in a similar way, considering contamination from  $^{A+2}_{Z+1}\text{X}$  nuclei. In this way the actual number of implanted ions,  $N_{imp}$ , is obtained, with relative uncertainties increasing as  $Z$  decreases. The position of the different species obtained with the above method agrees well with the MOCADI calculations.

#### D. Theoretical isomeric ratio

The projectile fragmentation process can be described with the so-called abrasion-ablation model. In the initial abrasion phase, a hot prefragment is created by removing a number of nucleons from the projectile. In the subsequent ablation phase, the highly excited prefragment evaporates nucleons until the final fragment is formed with an excitation energy below the particle emission threshold. A statistical  $\gamma$ -ray cascade then proceeds down to the yrast line and along this line to the ground state. If a long-lived state lies on this decay path, part of the cascade may be hindered or stopped depending on the lifetime of the isomer. The isomeric ratio is equal to the probability that the  $\gamma$  decay from the initial excited fragments proceeds via this isomeric state.

The Monte Carlo code ABRABLA [23] can be applied to describe the angular momentum distribution of the fragment. Furthermore, it has been shown that for a large mass difference between the projectile and the fragment this distribution can be approximated by a simple analytical formula [24]:

$$P_I = \frac{2I+1}{2\sigma_f^2} \exp\left[-\frac{I(I+1)}{2\sigma_f^2}\right], \quad (7)$$

where  $\sigma_f$ , the so-called spin-cutoff parameter of the final fragments, is given by

$$\sigma_f^2 = \langle j_z^2 \rangle \frac{(A_p - A_f)(\nu A_p + A_f)}{(\nu + 1)^2 (A_p - 1)}. \quad (8)$$

Here  $A_p$  and  $A_f$  are the projectile and fragment mass numbers, respectively,  $\nu$  is the mean number of evaporated nucleons per abraded mass unit, and  $\langle j_z^2 \rangle$  is the mean square angular momentum projection of a nucleon in the nucleus. It is generally assumed that the abrasion of a nucleon induces an excitation energy of about 27 MeV [25], whereas the evaporation of a nucleon decreases the energy by about 13 MeV, hence the parameter  $\nu=2$  is taken. The value of  $\langle j_z^2 \rangle$  is estimated on the basis of a semiclassical consideration of the angular momentum distribution in the Woods-Saxon potential [24,26], and can be written as

$$\langle j_z^2 \rangle = 0.16A_p^{2/3} \left(1 - \frac{2}{3}\beta\right), \quad (9)$$

where  $\beta$  is the quadrupole deformation parameter of the fragment. As all nuclei in the present study are situated in the vicinity of the  $Z=82$  spherical shell closure, we use  $\beta=0$  for all cases. Given a certain angular momentum distribution of the final fragment, one can consider the probability that the  $\gamma$  decay will lead to a metastable state of spin  $I_m$ . The extreme simplifying assumption is made that all states with  $I \geq I_m$ , and only those, decay to the isomer. A similar approach, known in the literature as the ‘‘sharp cutoff model,’’ has been used in studies of angular momentum distributions in compound nuclei [27–29] and in fission fragments [30]. From Eq. (7) we have the following equation:

$$\rho_{th} = \int_{I_m}^{\infty} P_I dI = \exp\left[-\frac{I_m(I_m+1)}{2\sigma_f^2}\right]. \quad (10)$$

Substituting  $\nu=2$ ,  $\beta=0$ , and introducing  $\Delta A = A_p - A_f$ , Eqs. (8) and (9) yield

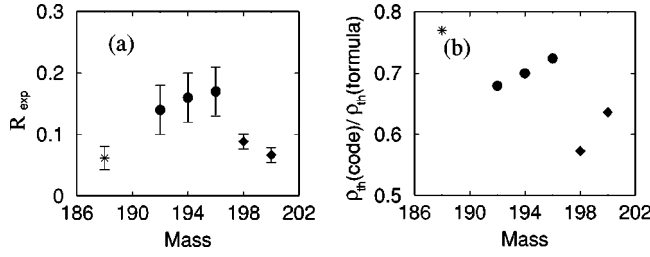


FIG. 5. (a) Experimental isomeric ratios for the  $12^+$  isomers in  $^{188}\text{Hg}$  (represented by a star),  $^{192,194,196}\text{Pb}$  (circle), and  $^{198,200}\text{Po}$  (diamond). (b) The ratio of the isomeric ratios calculated using the ABRABLA code and the analytical formula for the same isomers.

$$\sigma_f^2 = 0.0178 A_p^{2/3} \frac{\Delta A(3A_p - \Delta A)}{A_p - 1}. \quad (11)$$

#### IV. RESULTS

Isomeric decays associated with  $^{188}\text{Hg}$ ,  $^{192}\text{Tl}$ ,  $^{192,193,194,195,196}\text{Pb}$ ,  $^{195,196}\text{Bi}$ , and  $^{198,200,202}\text{Po}$  nuclei were observed. Preliminary results were reported in Refs. [31,32]. Delayed  $\gamma$ -ray energy spectra, as well as time spectra, are presented in Fig. 3. All the isomers observed in the present measurement were already reported from experiments using fusion-evaporation reactions. Therefore their properties (spin-parity, lifetimes,  $\gamma$ -ray energies, and multiplicities) are reasonably well known; this is important for the isomeric ratio determination.

The experimentally determined and theoretical isomeric ratios are summarized in Table I. In addition, the lifetimes from the literature are compared with those determined from the present experiment. Our lifetimes are in agreement with those from the literature, but have larger uncertainties, and therefore the previously published lifetimes were used for the isomeric ratio determination. There are six isomeric states with spin parity  $I^\pi=12^+$  observed in the present work, and their isomeric ratios as a function of mass are plotted in Fig. 5(a).

The isomeric ratios given in Table I were determined by using all possible  $\gamma$ -ray transitions with energies higher than 200 keV. Generally, transitions below 200 keV were not used because of the large uncertainties in the  $\gamma$ -ray detection efficiency due to the wide variation in depth of implantation

inside the catcher. The errors on the isomeric ratios are in the range of 10–30%. They are dominated by uncertainties in the number of implanted ions (10–15% uncertainty), the  $\gamma$ -ray detection efficiency ( $\approx 10\%$ ), and the statistical uncertainties in the number of counts in the  $\gamma$ -ray lines ( $\approx 10\%$ ).

In some cases, specifically  $^{192}\text{Tl}$ ,  $^{195,197}\text{Bi}$ ,  $^{198}\text{Po}$ , and  $^{200}\text{Po}$ , the energy of the transition directly depopulating the isomer is unknown. However, they are known to be low energy transitions below 50 keV [34,37,39–41,43,44]. (Note that the energy of the isomeric state in  $^{193}\text{Pb}$  is not known since the energy of the low-lying  $13/2^+$  state, on which the high-spin structure is built, is unknown compared to the ground state [35].) In  $^{202}\text{Po}$  the energy of the transition depopulating the ( $8^+$ ) isomer is tentatively known to be of 22 keV [42]. The number of decays during the flight time through the FRS depends on the energies of the depopulating transitions through the internal conversion coefficients. Therefore the value of the extracted isomeric ratio also depends on the energy of the depopulating transition. For all the above listed isomers the isomeric ratios were determined for the two extreme assumptions, considering 0 keV (no decay in flight through the FRS) and 50 keV depopulating  $\gamma$  rays. As one can see from the values given in Table II, the isomeric ratios are generally insensitive to the energies of the depopulating transitions. Exceptions are  $^{195,197}\text{Bi}$ , where the depopulating transition of the  $I^\pi=(29/2^-)$  isomers has an  $E1$  character, resulting in a large difference between  $\alpha(50 \text{ keV})=0.6$  and  $\alpha(0 \text{ keV})=\infty$ .

As mentioned previously, in the identification plot the  ${}^A_Z X$  nuclei were contaminated with  ${}^{A+2}_{Z+1} Y$  ions. In the cases of some well populated isomers, the isomeric ratio could be determined even when the ions were transmitted as contaminants. The obtained values from both the  $Z$  and  $Z-1$  gated identifications are given in Table III. Generally there is a good agreement between the two values, with the exception of the  $^{192}\text{Tl}$  and  $^{194}\text{Pb}$  isomers. The discrepancies for these two nuclei are probably related to their trajectories, which are very close to the edge of the spectrometer [see Figs. 4(e)–4(g)], meaning that their spatial distributions do not have a Gaussian shape. The adopted isomeric ratios given in Table I are the averaged values.

#### V. DISCUSSION

Isomeric ratios were calculated using both the ABRABLA code and the simple analytical formula. It was previously

TABLE II. Isomeric ratio for isomers where the exact energy of the first depopulating  $\gamma$ -ray transition is unknown. Values extracted for the two extreme cases,  $E_\gamma=0 \text{ keV}(\alpha=\infty)$  and  $E_\gamma=50 \text{ keV}$ , are given.

Isotope	$I^\pi$	$E_{lev}$ (keV)	$R_{exp}$ ( $E_\gamma=50 \text{ keV}$ )	$R_{exp}$ ( $E_\gamma=0 \text{ keV}$ )
$^{192}\text{Tl}$	( $8^-$ )	$407+x$	0.23 (10)	0.22 (10)
$^{195}\text{Bi}$	( $29/2^-$ )	$2311+x$	0.048 (8)	0.43 (7)
$^{197}\text{Bi}$	( $29/2^-$ )	$2360+x$	0.094 (18)	0.068 (13)
$^{198}\text{Po}$	$12^+$	$2692+x$	0.089 (12)	0.089 (12)
$^{200}\text{Po}$	( $12^+$ )	$2805+x$	0.067 (12)	0.067 (12)
	$11^-$	2597	0.393 (41)	0.393 (41)
$^{202}\text{Po}$	( $8^+$ )	(1714)	0.045 (12)	0.044 (12)

TABLE III. Isomeric ratios as determined from gates on  $Z$  and  $Z-1$ . See the text for details.

Isotope	$I^\pi$	$E_{lev}$ (keV)	$R_{exp}$ (gate on $Z$ )	$R_{exp}$ (gate on $Z-1$ )
$^{192}\text{Tl}$	(8 <sup>-</sup> )	407+x	0.291(48)	0.152(33)
$^{192}\text{Pb}$	(12 <sup>+</sup> )	2625	0.153(27)	0.136(28)
$^{194}\text{Pb}$	(12 <sup>+</sup> )	2629	0.189(23)	0.133(18)
$^{195}\text{Bi}$	(29/2 <sup>-</sup> )	2311+x	0.042(8)	0.049(10)
$^{196}\text{Pb}$	(12 <sup>+</sup> )	2694	0.182(42)	0.168(46)
	(5 <sup>-</sup> )	1798	0.37(18)	0.80(26)

shown that for near stable nuclei the approximate formula reproduces the angular momentum distribution predicted by the ABRABLA code rather well if the mass difference between projectile and fragment is greater than 10 mass units [4]. However, in the current-neutron deficient case, the situation is somewhat different, with the analytical formula predicting much higher angular momenta than the ABRABLA code [see Table I and Fig. 5(b)]. (We note that for neutron-rich nuclei the analytical formula systematically underestimates the isomeric ratios [45].)

The predictions of the analytical formula are based on the number of nucleons removed from the projectile in the abrasion step of the reaction. Since only the entire mass loss of the projectile is directly observed, the number of abraded nucleons can be estimated after assuming that the abrasion of one nucleon is followed by the evaporation of another two. As mentioned previously, this relation is applied by choosing  $\nu=2$ , but since  $\nu$  represents a mean number, case-dependent deviations from that rule can be expected. The production of neutron-deficient nuclei some way from the stability line requires larger numbers of nucleons lost from the projectile, which is achievable in long evaporation cascades. An increased mass loss during evaporation requires higher excitation energies of the nucleus, which remains after abrasion. This condition can be fulfilled if more strongly bound nucleons occupying low-lying single-particle states are removed. However, according to the predictions of the shell model, low-lying single-particle states possess lower angular momenta, compared to the angular momenta of all occupied single-particle states of the projectile nucleus. Consequently the required abrasion of low-lying nucleons for the production of exotic nuclei will imply the creation of hole states of low angular momenta and the resulting spin of the prefragment will be also decreased. The interplay between the excitation energy and the spin of the prefragment is treated in the ABRABLA code, but it is not explicitly incorporated into the analytical formula. As shown in Fig. 5(b), the differences appear to increase for more “exotic” nuclei. Since the ABRABLA code should give more reliable results than the analytical approximation, we compare the experimental values with its predictions.

The experimental isomeric ratios are generally smaller than the calculated values, as shown in Table I and Fig. 6(a). To understand this discrepancy we have taken a closer look at the assumption used in the calculations, namely, that all the states with spin  $I > I_m$  decay into the isomeric state (sharp cutoff approximation). It should also be pointed out that in cases where more than one isomer were observed in a given

nucleus, the isomeric ratios obtained experimentally for the lower-lying states cannot be compared directly with the model because its assumption that all states with the higher spin decay promptly to the isomer of interest is explicitly violated. In these cases the  $\rho_{thL} - b_{UL}\rho_{thU}$  quantity should be compared with the experimental value. Nevertheless, in the following we do not discuss the population of the lower-lying isomeric states, since they are a less sensitive probe of the theory than the higher-spin isomers.

One might expect that the sharp cutoff approximation would be justified only for isomers lying close to the yrast line and the isomeric ratio should decrease with increasing excitation energy of an isomer above the yrast line. Such a tendency was indeed observed, as described in Ref. [4]. In our case all the isomers correspond to yrast states, with only one exception: the  $21/2^-$  isomer in  $^{195}\text{Pb}$  lies 5 keV higher than a  $21/2^+$  state. However, even in the case of yrast isomers, there might be transitions from higher-lying states by-passing the isomer and therefore reducing the isomeric ratio. The effect of these bypassing transitions can be taken into account as follows. The near yrast structures of several nuclei studied in the present work are well known from studies using fusion-evaporation reactions with heavy-ion beams. These reactions are somewhat similar to projectile fragmentation with a large mass difference between fragment and projectile, in the sense that they both populate states close to the yrast line. Therefore the fraction  $\varphi$  of intensity passing through the isomer as compared to the total intensity at that excitation energy determined from fusion-evaporation reactions can be used to correct the isomeric ratio:  $\rho_{exp} = R_{exp} / \varphi$ . The quantity  $\rho_{exp}$  gives the probability of populating states with higher angular momentum than the isomer and can be directly compared with the theory. For  $\rho$  in the following we

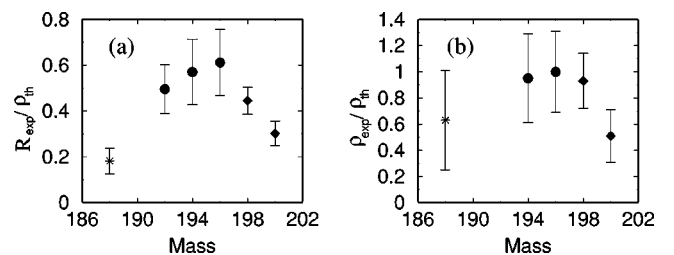


FIG. 6. (a) The ratio of the experimental and theoretical (ABRABLA in the sharp cutoff approximation) isomeric ratios for the  $12^+$  isomeric states in  $^{188}\text{Hg}$  (represented by a star),  $^{192,194,196}\text{Pb}$  (circle), and  $^{198,200}\text{Po}$  (diamond). (b) Ratio of the experimental and theoretical angular-momentum population for spin 12 in the same nuclei.

TABLE IV. Comparison of experimental and theoretical angular-momentum populations. For details see the text.

Isotope	$I^\pi$	$R_{exp}$	$\varphi$	$\rho_{exp}$	$\rho_{th}$	$\rho_{exp}/\rho_{th}$
$^{188}\text{Hg}$	(12 <sup>+</sup> )	0.062 (19)	0.29 (15) [48]	0.21 (13)	0.341	0.63 (38)
$^{193}\text{Pb}$	(33/2 <sup>+</sup> )	0.015 (4)	0.11 (2) [49]	0.14 (4)	0.113	1.21 (39)
$^{194}\text{Pb}$	(12 <sup>+</sup> )	0.16 (4)	0.60 (15) [50]	0.27 (9)	0.280	0.95 (34)
$^{196}\text{Pb}$	(12 <sup>+</sup> )	0.17 (4)	0.61 (12) [33]	0.28 (9)	0.278	1.00 (31)
$^{197}\text{Bi}$	(29/2 <sup>-</sup> )	0.08 (2)	0.47 (14) [44]	0.17 (7)	0.165	1.03 (40)
$^{198}\text{Po}$	12 <sup>+</sup>	0.089 (12)	0.48 (9) [51]	0.19 (4)	0.200	0.93 (21)
$^{200}\text{Po}$	(12 <sup>+</sup> )	0.067 (12)	0.60 (20) [52]	0.11 (4)	0.222	0.51 (20)

use the term “angular momentum population” to refer to the fractional population at and above a specified spin value. The factors  $\varphi$  and  $\rho_{exp}$  are given in Table IV. The accuracy of  $\varphi$  depends on the sensitivity of a given experiment, more sensitive experiments tending to lead to lower  $\varphi$  values. The uncertainties on  $\varphi$  indicated in Table IV have been increased relative to the statistical value to take account of uncertainties in the level scheme.

There are not sufficient experimental data on the level schemes of  $^{192}\text{Tl}$ ,  $^{195}\text{Bi}$ ,  $^{202}\text{Po}$  around the isomers, so the angular-momentum population in these ions cannot be compared directly with the theory. We note that in  $^{202}\text{Po}$  there is a higher-lying 11<sup>-</sup> isomeric state with a lifetime  $T_{1/2} > 200$  ns [42], which may be responsible for the lower than predicted isomeric ratio of the 8<sup>+</sup> state in this nucleus. The situation might be similar in  $^{195}\text{Bi}$  in which three new transitions were observed (see Fig. 3). These  $\gamma$  rays might be related to a higher-lying isomeric state of which decay into the (29/2<sup>-</sup>) isomer could explain the very low isomeric ratio. Although the level scheme of  $^{192}\text{Pb}$  is well known, the intensity relation between the transitions feeding the isomer and bypassing the isomer is not known [46], so the factor  $\varphi$  could not be determined.

The theoretical angular momentum population can be compared with the experimental values in  $^{188}\text{Hg}$ ,  $^{193,194,196}\text{Pb}$ ,  $^{197}\text{Bi}$ , and  $^{198,200}\text{Po}$  (see Table IV). The agreement between theory and experiment is very good for  $^{193,194,196}\text{Pb}$ ,  $^{197}\text{Bi}$ , and  $^{198}\text{Po}$ . Within the error limit there is also agreement for  $^{188}\text{Hg}$ . However, the population of the 12<sup>+</sup> isomeric state in  $^{200}\text{Po}$  is only half of the calculated value. Insufficient knowledge of its level scheme might be the reason for this discrepancy. Indeed, the data imply the existence of another isomer.

One can note the large number of 12<sup>+</sup> isomers observed in the present experiment, namely, in  $^{188}\text{Hg}$ ,  $^{192,194,196}\text{Pb}$ , and  $^{198,200}\text{Po}$  nuclei. All these states are spherical with  $\nu i_{13/2}^{-2}$  configuration, except in  $^{188}\text{Hg}$  where the 12<sup>+</sup> isomer was alternatively interpreted as member of an oblate band [47]. The related structures of these isomeric states are reflected in their similar  $\varphi$  value, as determined for  $^{194,196}\text{Pb}$  and  $^{194,200}\text{Po}$ . As we mentioned earlier,  $\varphi$  could not be determined for  $^{192}\text{Pb}$ , but assuming a similar value as for the other heavier lead isotopes ( $\varphi=0.6$ ), a good agreement with the theory is obtained, namely,  $\rho_{exp}/\rho_{th}=0.83$ .

It can be inferred that there is good agreement between the calculated and experimental angular momentum populations. The experimental value was determined from the isomeric ratio by taking into account the decay properties of the higher-lying states. Although, an assumption on the angular momentum population was already used when estimating this correction factor, the overall agreement can be considered as an indication that this presupposition was appropriate. We note that in previous studies no such correction was applied [3,4]. Nevertheless in the case of yrast isomers a reasonable agreement with the theory was found. However, the absence of suitable data from which to obtain the corresponding correction factors makes it difficult to explore this surprising feature.

## VI. CONCLUSIONS

Approximately 15 previously known isomeric states in the neutron-deficient  $A \approx 190$  region were identified following the projectile fragmentation of a 750A MeV  $^{238}\text{U}$  beam. The deduced isomeric ratios are smaller than those calculated with the ABRABLA code based on the abrasion-ablation model of fragmentation including the sharp cutoff approximation. Reasonable agreement can be obtained between the experimental and calculated angular-momentum populations by correcting the isomeric ratios with a factor which reflects the decay pattern of the states above the isomer. This improved understanding of the angular-momentum distributions in exotic nuclei formed via the projectile fragmentation technique may be important for future studies with radioactive beams.

## ACKNOWLEDGMENTS

The excellent work of the FRS technical staff and the accelerator group at GSI is acknowledged. This work was supported by EPSRC(UK), the EU Access to Large Scale Facilities Programme, and the EU Fifth Framework Programme “EXOTAG” (Contract No. HPRI-1999-CT-50017). Zs.P. acknowledges the financial support from EPSRC (Grant No. GR/A10789/01).

- [1] W.-D. Schmidt-Ott, K. Asahi, Y. Fujita, H. Geissel, K.-D. Gross, T. Hild, H. Irmich, M. Ishihara, K. Krumbholz, V. Kunze, A. Magel, F. Meissner, K. Muto, F. Nickel, H. Okuno, M. Pfützner, C. Scheidenberger, K. Suzuki, M. Weber, and C. Wennemann, *Z. Phys. A* **350**, 215 (1994).
- [2] R. Grzywacz, R. Anne, G. Auger, D. Bazin, C. Borcea, V. Borrel, J. M. Corre, T. Dörfler, A. Fomichov, M. Gaelens, D. Guillemaud-Mueller, R. Hue, M. Huyse, Z. Janas, H. Keller, M. Lewitowicz, S. Lukyanov, A. C. Mueller, Yu. Penionzhkevich, M. Pfützner, F. Pougheon, K. Rykaczewski, M. G. Saint-Laurent, K. Schmidt, W.-D. Schmidt-Ott, O. Sorlin, J. Szerypo, O. Tarasov, J. Wauters, and J. Zylicz, *Phys. Lett. B* **355**, 439 (1995).
- [3] M. Pfützner, P. Armbruster, T. Baumann, J. Benlliure, M. Bernas, W. N. Catford, D. Cortina-Gil, J. M. Daugas, H. Geissel, M. Górska, H. Grawe, R. Grzywacz, M. Hellström, N. Iwasa, Z. Janas, A. R. Junghans, M. Karny, S. Leenhardt, M. Lewitowicz, A. C. Mueller, F. de Oliveira, P. H. Regan, M. Rejmund, K. Rykaczewski, and K. Sümmerer, *Phys. Lett. B* **444**, 32 (1998).
- [4] M. Pfützner, P. H. Regan, P. M. Walker, M. Caamaño, J. Gerl, M. Hellström, P. Mayet, K.-H. Schmidt, Zs. Podolyák, M. N. Mineva, A. Aprahamian, J. Benlliure, A. M. Bruce, P. A. Butler, D. Cortina Gil, D. M. Cullen, J. Döring, T. Enqvist, C. Fox, J. Garcès Narro, H. Geissel, W. Gelletly, J. Giovinazzo, M. Górska, H. Grawe, R. Grzywacz, A. Kleinböhl, W. Korten, M. Lewitowicz, R. Lucas, H. Mach, C. D. O'Leary, F. De Oliveira, C. J. Pearson, F. Rejmund, M. Rejmund, M. Sawicka, H. Schaffner, Ch. Schlegel, K. Schmidt, Ch. Theisen, F. Vivès, D. D. Warner, C. Wheldon, H. J. Wollersheim, and S. Wooding, *Phys. Rev. C* **65**, 064604 (2002).
- [5] C. Chandler, P. H. Regan, C. J. Pearson, B. Blank, A. M. Bruce, W. N. Catford, N. Curtis, S. Czajkowski, W. Gelletly, R. Grzywacz, Z. Janas, M. Lewitowicz, C. Marchand, N. A. Orr, R. D. Page, A. Petrovici, A. T. Reed, M. G. Saint-Laurent, S. M. Vincent, R. Wadsworth, D. D. Warner, and J. S. Winfield, *Phys. Rev. C* **56**, R2924 (1997).
- [6] R. Grzywacz, R. Anne, G. Auger, C. Borcea, J. M. Corre, T. Dörfler, A. Fomichov, S. Grevy, H. Grawe, D. Guillemaud-Mueller, M. Huyse, Z. Janas, H. Keller, M. Lewitowicz, S. Lukyanov, A. C. Mueller, N. Orr, A. Ostrowski, Yu. Penionzhkevich, A. Piechaczek, F. Pougheon, K. Rykaczewski, M. G. Saint-Laurent, W.-D. Schmidt-Ott, O. Sorlin, J. Szerypo, O. Tarasov, J. Wauters, and J. Zylicz, *Phys. Rev. C* **55**, 1126 (1997).
- [7] Zs. Podolyák, P. H. Regan, M. Pfützner, J. Gerl, M. Hellström, M. Caamaño, P. Mayet, Ch. Schlegel, A. Aprahamian, J. Benlliure, A. M. Bruce, P. A. Butler, D. Cortina Gil, D. M. Cullen, J. Döring, T. Enqvist, F. Rejmund, C. Fox, J. Garcès Narro, H. Geissel, W. Gelletly, J. Giovinazzo, M. Górska, H. Grawe, R. Grzywacz, A. Kleinböhl, W. Korten, M. Lewitowicz, R. Lucas, H. Mach, M. Mineva, C. D. O'Leary, F. De Oliveira, C. J. Pearson, M. Rejmund, M. Sawicka, H. Schaffner, K. Schmidt, Ch. Theisen, P. M. Walker, D. D. Warner, C. Wheldon, H. J. Wollersheim, S. C. Wooding, and F. R. Xu, *Phys. Lett. B* **491**, 225 (2000).
- [8] C. Chandler, P. H. Regan, B. Blank, C. J. Pearson, A. M. Bruce, W. N. Catford, N. Curtis, S. Czajkowski, Ph. Dessagne, A. Fleury, W. Gelletly, J. Giovinazzo, R. Grzywacz, Z. Janas, M. Lewitowicz, C. Marchand, Ch. Miché, N. A. Orr, R. D. Page, M. S. Pravikoff, A. T. Reed, M. G. Saint-Laurent, S. M. Vincent, R. Wadsworth, D. D. Warner, J. S. Winfield, and F. Xu, *Phys. Rev. C* **61**, 044309 (2000).
- [9] M. N. Mineva, M. Hellström, M. Bernas, J. Gerl, H. Grawe, M. Pfützner, P. H. Regan, M. Rejmund, D. Rudolph, F. Becker, C. R. Bingham, T. Enqvist, B. Fogelberg, H. Gausemel, H. Geissel, J. Genevey, M. Górska, R. Grzywacz, K. Hauschild, Z. Janas, I. Kojouharov, Y. Kopatch, A. Korgul, W. Korten, J. Kurcewicz, M. Lewitowicz, R. Lucas, H. Mach, S. Mandal, P. Mayet, C. Mazzocchi, J. A. Pinston, Zs. Podolyák, H. Schaffner, Ch. Schlegel, K. Schmidt, K. Sümmerer, and H. J. Wollersheim, *Eur. Phys. J. A* **11**, 9 (2001).
- [10] T. Enqvist, J. Benlliure, F. Farget, K.-H. Schmidt, P. Armbruster, M. Bernas, L. Tassan-Got, A. Boudard, R. Legrain, C. Volant, C. Böckstiegel, M. de Jong, and J. P. Dufour, *Nucl. Phys. A* **658**, 47 (1999).
- [11] J. Benlliure, K.-H. Schmidt, D. Cortina-Gil, T. Enqvist, F. Farget, A. Heinz, A. R. Junghans, J. Pereira, and J. Taieb, *Nucl. Phys. A* **660**, 87 (1999).
- [12] K. Sümmerer and B. Blank, *Phys. Rev. C* **61**, 034607 (2000), and references therein.
- [13] H. Geissel, P. Armbruster, K. H. Behr, A. Brünle, K. Burkard, M. Chen, H. Folger, B. Franczak, H. Keller, O. Klepper, B. Langenbeck, F. Nickel, E. Pfeng, M. Pfützner, E. Roeckl, K. Rykaczewski, I. Schall, D. Schardt, C. Scheidenberger, K.-H. Schmidt, A. Schröter, T. Schwab, K. Sümmerer, M. Weber, G. Müntenberg, T. Brohm, H.-G. Clerc, M. Fauerbach, J.-J. Gaimard, A. Grewe, E. Hanelt, B. Knödler, M. Steiner, B. Voss, J. Weckenmann, C. Ziegler, A. Magel, H. Wollnik, J. P. Dufour, Y. Fujita, D. J. Vieira, and B. Sherrill, *Nucl. Instrum. Methods Phys. Res. B* **70**, 286 (1992).
- [14] Zs. Podolyák, P. H. Regan, P. M. Walker, M. Caamaño, P. Mayet, J. Gerl, Ch. Schlegel, M. Hellström, M. N. Mineva, and M. Pfützner, GSI ISOMER Collaboration, in *Proceedings of the conference "Exotic Nuclei at the Proton-Drip Line," Camerino, Italy, 2001*, edited by C. M. Petrache and G. Lo Bianco (University of Camerino, Camerino 2001), p. 189.
- [15] Zs. Podolyák, P. H. Regan, P. M. Walker, M. Caamaño, K. A. Gladnishi, J. Gerl, M. Hellström, P. Mayet, M. Pfützner, and M. Mineva, GSI ISOMER Collaboration, *Nucl. Phys. A* **722**, 237c (2003).
- [16] J. Gerl, *Nucl. Instrum. Methods Phys. Res. A* **442**, 238 (2000).
- [17] Zs. Podolyák, M. Caamaño, P. H. Regan, P. M. Walker, P. Mayet, J. Gerl, Ch. Schlegel, M. Hellström, M. N. Mineva, and M. Pfützner, GSI ISOMER Collaboration, *Prog. Theor. Phys. Suppl.* **146**, 467 (2002).
- [18] M. Caamaño, P. M. Walker, P. H. Regan, C. J. Pearson, Zs. Podolyák, P. Mayet, J. Gerl, Ch. Schlegel, M. Hellström, M. Mineva, and M. Pfützner, *Acta Phys. Pol. B* **32**, 763 (2001).
- [19] C. Scheidenberger, Th. Stölker, W. E. Meyerhof, H. Geissel, P. H. Mokler, and B. Blank, *Nucl. Instrum. Methods Phys. Res. B* **142**, 441 (1998).
- [20] E. Casarejos, Ph.D. thesis, University of Santiago de Compostella, Spain, 2002.
- [21] R. Anholt, Ch. Stoller, J. D. Molitoris, D. W. Spooner, E. Morenzoni, S. A. Andriamonje, W. E. Meyerhof, H. Bowman, J.-S. Xu, Z.-Z. Xu, J. O. Rasmussen, and D. H. H. Hoffmann, *Phys. Rev. A* **33**, 2270 (1986); H. Tawara, T. Azuma, T. Ito, K. Komaki, Y. Yamazaki, T. Matsuo, T. Tonuma, K. Shima, A. Kitagawa, and E. Takada, *ibid.* **55**, 808 (1997).

- [22] N. Iwasa, H. Geissel, G. Münzenberg, C. Scheidenberger, Th. Schwab, and H. Wollnik, *Nucl. Instrum. Methods Phys. Res. B* **126**, 284 (1997).
- [23] J.-J. Gaimard and K.-H. Schmidt, *Nucl. Phys.* **A531**, 709 (1991).
- [24] M. de Jong, A. V. Ignatyuk, and K.-H. Schmidt, *Nucl. Phys.* **A613**, 435 (1997).
- [25] K.-H. Schmidt, T. Brohm, H.-G. Clerc, M. Dornik, M. Fauerbach, H. Geissel, A. Grewe, E. Hanelt, A. Junghans, A. Magel, W. Morawek, G. Münzenberg, F. Nickel, M. Pfützner, C. Scheidenberger, K. Sümmerer, D. Vieira, B. Voss, and C. Ziegler, *Phys. Lett. B* **300**, 313 (1993).
- [26] A. V. Ignatyuk, *Statistical Properties of Excited Nuclei* (Energoatomizdat, Moscow, 1983) (Russian).
- [27] J. R. Huizenga and R. Vandenbosch, *Phys. Rev.* **120**, 1305 (1960).
- [28] R. Vandenbosch and J. R. Huizenga, *Phys. Rev.* **120**, 1313 (1960).
- [29] I. S. Grant and M. Rathle, *J. Phys. G* **5**, 1741 (1979), and references therein.
- [30] H. Naik, S. P. Dange, R. J. Singh, S. K. Das, and R. Guin, *Nucl. Phys.* **A648**, 45 (1999), and references therein.
- [31] K. A. Gladnishki, Zs. Podolyák, J. Gerl, M. Hellström, Y. Kopatch, S. Mandal, M. Górska, P. H. Regan, H. J. Wollersheim, A. Banu, G. Benzoni, H. Boardman, M. La Commara, J. Ekman, C. Fahlander, H. Geissel, H. Grawe, E. Kaza, A. Korgul, M. Matos, M. Mineva, R. Page, C. J. Pearson, C. Plettner, D. Rudolph, Ch. Scheidenberger, V. Shishkin, D. Sohler, K. Sümmerer, J. J. Valiente Dobon, H. Weick, and M. Winkler, *Acta Phys. Pol. B* **34**, 2395 (2003).
- [32] Zs. Podolyák, K. A. Gladnishki, J. Gerl, M. Hellström, Y. Kopatch, S. Mandal, M. Górska, P. H. Regan, H. J. Wollersheim, K.-H. Schmidt, and O. Yordanov, *GSI-ISOMER Collaboration, Proceedings of the International Conference on the Labyrinth in Nuclear Structure, Crete, Greece, 2003*.
- [33] A. K. Singh, N. Nenoff, D. Roßbach, A. Görge, S. Chmel, F. Azaiez, A. Astier, D. Bazzacco, M. Bellegruic, S. Bouneau, C. Bourgeois, N. Buforn, B. Cederwall, I. Deloncle, J. Domscheit, F. Hannachi, K. Hauschild, H. Hübel, A. Korichi, W. Korten, T. Kröll, Y. LeCoz, A. Lopez-Martens, R. Lucas, S. Lunardi, H. J. Maier, E. Mergel, M. Meyer, C. M. Petrache, N. Redon, P. Reiter, C. Rossi-Alvarez, G. Schönwaßer, O. Stezowski, P. G. Thirolf, and A. N. Wilson, *Nucl. Phys.* **A707**, 3 (2002).
- [34] C. M. Baglin, *Nucl. Data Sheets* **84**, 717 (1998).
- [35] A. A. Cohen, *Nucl. Data Sheets* **83**, 921 (1998).
- [36] E. Browne and B. Singh, *Nucl. Data Sheets* **79**, 277 (1996).
- [37] Z. Chunmei, *Nucl. Data Sheets* **86**, 645 (1999).
- [38] Z. Chunmei, W. Gongqing, and T. Zhenlan, *Nucl. Data Sheets* **83**, 145 (1998).
- [39] Z. Chunmei, *Nucl. Data Sheets* **76**, 399 (1995).
- [40] C. Zhou, *Nucl. Data Sheets* **95**, 59 (2002).
- [41] M. R. Schmorak, *Nucl. Data Sheets* **75**, 667 (1995).
- [42] M. R. Schmorak, *Nucl. Data Sheets* **80**, 647 (1997).
- [43] T. Lönnroth, C. W. Beausang, D. B. Fossan, L. Hildingsson, W. F. Piel, Jr., M. A. Quader, S. Vajda, T. Chapuran, and E. K. Warburton, *Phys. Rev. C* **33**, 1641 (1986).
- [44] T. Chapuran, K. Dybdal, D. B. Fossan, T. Lönnroth, W. F. Piel, Jr., D. Horn, and E. K. Warburton, *Phys. Rev. C* **33**, 130 (1986).
- [45] M. Caamaño *et al.* (in preparation).
- [46] A. J. M. Plompen, M. N. Harakeh, W. H. A. Hesselink, G. van't Hof, N. Kalantar-Nayestanaki, J. P. S. van Schagen, M. P. Carpenter, I. Ahmad, I. G. Bearden, R. V. F. Janssens, T. L. Khoo, T. Lauritsen, Y. Liang, U. Garg, W. Reviol, and D. Ye, *Nucl. Phys.* **A562**, 61 (1993).
- [47] B. Singh, *Nucl. Data Sheets* **95**, 387 (2002).
- [48] F. Hannachi, G. Bastin, M. G. Porquet, C. Schück, J. P. Thibaud, C. Bourgeois, L. Hildingsson, D. Jerrestam, N. Perrin, H. Sergolle, F. A. Beck, T. Byrski, J. C. Merdinger, and J. Dudek, *Nucl. Phys.* **A481**, 135 (1988).
- [49] G. Baldsiefen, M. A. Stoyer, J. A. Cizewski, D. P. McNabb, W. Younes, J. A. Becker, L. A. Bernstein, M. J. Brinkman, L. P. Farris, E. A. Henry, J. R. Hughes, A. Kuhnert, T. F. Wang, B. Cederwall, R. M. Clark, M. A. Deleplanque, R. M. Diamond, P. Fallon, I. Y. Lee, A. O. Macchiavelli, J. Oliveira, F. S. Stephens, J. Burde, D. T. Vo, and S. Frauendorf, *Phys. Rev. C* **54**, 1106 (1996).
- [50] M. Kaci, M.-G. Porquet, I. Deloncle, M. Aiche, F. Azaiez, G. Bastin, C. W. Beausang, C. Bourgeois, R. M. Clark, R. Duffait, J. Duprat, B. J. P. Gall, F. Hannachi, K. Hauschild, M. J. Joyce, A. Korichi, Y. Le Coz, M. Meyer, E. S. Paul, N. Perrin, N. Poffé, N. Redon, C. Schück, H. Sergolle, J. F. Sharpey-Schafer, J. Simpson, A. G. Smith, and R. Wadsworth, *Nucl. Phys.* **A697**, 3 (2002).
- [51] A. Maj, H. Grawe, H. Kluge, A. Kuhnert, K. H. Maier, J. Recht, N. Roy, H. Hübel, and M. Guttormsen, *Nucl. Phys.* **A509**, 413 (1990).
- [52] T. Weckström, B. Fant, T. Lönnroth, V. Rahkonen, A. Källberg, and C. J. Herrlander, *Z. Phys. A* **321**, 231 (1985).